Investigation of CuIn$_{1-x}$Ga$_x$Se$_2$ thin films co-evaporated from two metal sources for photovoltaic solar cells

A. BOURAOUI[a], Y. BERREDJEM[b], A. AIN-SOUYA[c], A. DRICI[a*], A. AMARA[a], M. KANZARI[d],
F. CHAFFAR AKKARI[d], N. KHEMIRI[d], J. C. BERNEDE[e]
[a]LEREC, Département de Physique, Université Badji Mokhtar Annaba, BP 12 Annaba, Algeria
[b]LTE,Université Mohamed Cherif Mesaidia, Souk-Ahras, Algeria
[c]LESIMS, Département de Physique, Université Badji Mokhtar Annaba, BP 12 Annaba, Algeria
[d]LPMS, Ecole Nationale d'Ingénieurs de Tunis (ENIT), BP 37, Tunis Belvédère 1002, Tunisie
[e]MOLTECH(Anjou), 2 Rue de la Houssinière, BP 92208, 44322 Nantes Cedex, France

CuIn$_{1-x}$Ga$_x$Se$_2$ (CIGS) thin films were grown by co-evaporation using two sources for the metal elements (Cu, Ga and In). A Mo coated soda lime glass substrates heated at 500 °C was used for the deposition. X-ray diffraction (XRD) and scanning electron microscopy (SEM) confirm that these films are polycrystalline with a chalcopyrite structure and showed homogeneous grain size estimate about 25 nm. X-ray photoelectron spectroscopy (XPS) was performed to analyse the binding energy values of Ga3d and O1s onto CIGSe layers. The conductivity measurements in the temperature range of 40-400 K were carried out for $0.05 \leq x \leq 0.23$. The effect of grain boundary scattering on the electrical transport played an important role in describing the transport processes in these films. The bowing factor is discussed taking into account the deposition techniques of CIGS films. It has been noticed that the open circuit voltage (V$_{oc}$) is influenced by Ga content and the energy gap value of the absorber CIGS thin layers and yielded a poor efficiency of solar cells.

1. Introduction

Solar cells based on Cu(In,Ga)Se$_2$ (CIGS) thin films have emerged as a leading candidate for low cost solar electric power generation. The Cu(In,Ga)Se$_2$ band gap (Eg) can be increased to match the solar spectrum for higher efficiency by alloying the group III or VI elements[1-6]. The Cu(In,Ga)Se$_2$ thin film absorber solar cells allows to achieve high efficiency (20.8 %)in laboratory [7]. A comparative study of some physical properties of CIGS absorbers was presented as a function of preferred orientation, namely <112>- and <220/204>- oriented CIGS samples [8]. It is found that there are significant physical differences (e.g., morphology, defect formation, density of structural defects, optoelectronic) between materials of nominally the same atomic composition but with different preferred orientation. Such record cells are grown with the help of the three stage process using Knudsen effusion cells [5]. Less performing but cheaper cells can be grown by using simple classical tungsten source. However, during the co-evaporation, it is not easy to supervise the three simple metal evaporation sources in sequence required by the three stage process. Therefore, our contribution in this paper we describe the co-evaporation method using two simple sources for the metal elements and investigate some principal characterizations of polycrystalline p-CuIn$_{1-x}$GaSe$_2$ thin films using as the absorber layer in solar cells.

2. Experimental procedure

It consists to evaporate Cu, In, Ga and Se pure elements (99.99%) through a three-stage process using two metal sources of tungsten onto glass (SLG) substrates coated with molybdenum (Mo) and heated at 500 °C. The whole deposition time was 25 min. The CIGS films were 1.5µm thick. Different combination of the metal sources has been tested using three and two metal sources like: Cu +Ga, Cu + In, Se. Details of the CIGS preparation procedure is described elsewhere [9]. The Mo films were sputtered from a molybdenum target foil (diameter 75 mm, thickness 0.25 mm) [10] . In order to complete the device structure, a buffer layer of n-In$_2$S$_3$ was deposited by a PVD method. The deposition process of this buffer layer has been described precisely in ref.[11]. After the buffer evaporation, the ZnO layers were deposited using an rf magnetron sputtering system. A first thin no-conductive ZnO film (ZnO) was sputtered using a ZnO (2% Al$_2$O$_3$) target and an Ar+2% O$_2$ gas. Then the ZnO:Al conductive layer was deposited using the same crucible but in pure Ar sputtering gas. The conductivity of this ZnO:Al doped film was about: $\sigma = 2.10^3$ $(\Omega.cm)^{-1}$. To complete the cells, NiCr/Al grids were deposited at the top of the devices.

The films have been characterized by X-ray diffraction (XRD) by means of a Siemens D-500 diffractometer using the CuKα_1 radiation source (λ=0.15406 nm) (Institut des Matériaux de Nantes). The surface morphology were observed with a field effect scanning electron microscope (SEM) JEOL-F6400. Electron probe microanalysis (EPMA) were performed using a JEOL-F5800 LV scanning electron microscope

equipped with a Princeton Gamma-Tech (PGT) microanalysis system, in which X-rays were detected by a germanium crystal (Centre de microcaractérisation, Université de Nantes).

X-ray photoelectron spectroscopy (XPS) analyses were performed with Leybold LHS-12 apparatus. The data were obtained with a magnesium source of radiation (1253.6 eV) operating at 10kV and 10 mA. The energy resolution was 1 eV at pass energy of 50 eV. High resolution scans were obtained in the Ga3p and O1s region of the spectrum. The quantitative XPS studies were based on the determination of the peak areas with respectively 5.3, 3.8, 0.59, 0.58, 4.1 and 0.6 as sensitivity factors (the sensibility factors are given by the manufacturer, Leybold). The samples were grounded with silver paste to decrease the charge effect.

The depth profile was studied by recording successive XPS spectra obtained after argon ions etching. Etching was accomplished at pressures lower than 5×10^{-4} Pa, a 10mA emission current and a 5kV beam energy using an ion gun. The Ar^+ ions could etch the entire sample surface. Using these etching conditions the etching rate has been estimated to be 6.5 nm.s^{-1}. Electrical characterizations were preformed with an automated I-V tester under 1 sun global AM 1.5 simulated solar illuminations.

3. Results and discussion

3.1. Structure and morphology of CIGS thin films

In Fig. 1, we present typical X-ray diffraction spectra for three CuIn$_{1-x}$Ga$_x$Se$_2$ thin films x=0 (CuInSe$_2$), x= 0.2 (CIGS) and x=1(CuGaSe$_2$). The XRD indicated a strong reflection from (112) plan followed by (220/204) and (116/312) peaks. It is noted, there are no peaks visible after 2teta =60 ° as mentioned by JI et al. [12]. This confirmed that in the coevaporation process the temperature is higher and the InxSe phase is completely dissolved. The (101), (103) and (211) diffraction peaks visible in the spectra are typical of the chalcopyrite structure, which testify that the films are crystallized in the expected structure are in good agreement with JCPD cards No 87-2265. It is reported by several authors [13-14] this structure is necessary to obtain good quality solar cells

with high efficiency. In our study of CIGS thin films, we don't observe XRD peak ratio namely <220/204> over <112> estimate by Miguel A. Contreras et al. [8] of 1.94. Always, the <112> is much more accentuated than <220/204> peak. A shift of the peaks is observed when x varies from 0(CuInSe$_2$) to 1(CuGaSe$_2$). This behaviour shows that the lattice parameters a and c follows the Vergard's Law [9].
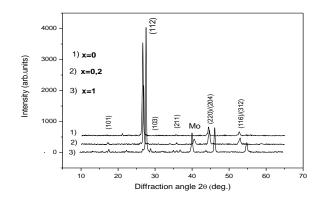

Fig. 1. X-ray diffraction diagram of CIGS thin films versus composition for (x = 0, 1and 0.2)

We reported in Fig. 2 a), b); SEM micrograph of typical CIGS thin films for two compositions $x = \frac{Ga}{(Ga+In)} = 0.23$ and 0.05 with predominant polycrystalline texture. The composition of this layer was determined from EPMA. The grain size D was calculate from Debye-Scherrer formula $D = \frac{K\lambda}{\beta \cos(\theta)}$ Where K=0.9 when β is estimate from the full width at half maximum (FWHM) of the peak (112) and λ is the wavelength of the X-rays. The typical value of grain size for these films is 250 nm. As visible by SEM micrograph, the grains are homogenous and confirm this size. Usually, we try to use a Cu evaporation rate which allows achieving Cu rich compound during the first part of the coevaporation. The Cu rich phase induces the presence of liquid Cu$_{2-x}$Se phase, which facilitates the growth of large CIGS grains [15].

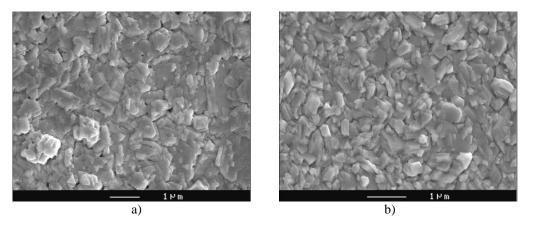a)   b)

Fig. 2. Microphotography of CIGS film deposited by two metal sources a) x=0.05, b) x=0.23

In order to control the Ga composition and the oxygen contamination through the CIGS thin films obtain by the coevaporation using three and four metal sources, we scan the surface and the bulk of the samples by XPS. Fig. 3a shows the Ga3p signal before and after three minutes of etching. We can see, that the signal exhibits a doublet at 105.80 and 105 eV. The area ratio between these peaks is

fixed equal to 0.80 eV. This implies that the Ga is associated to the metal elements In or Se. Before etching, only one peak of Ga3p at 105.8 eV is present. On the surface, the Ga was as Ga_2O_3 [16]. In fact, the surface is very contaminating with oxygen indicated by a strong signal at 532 eV as visible in Fig. 3c.
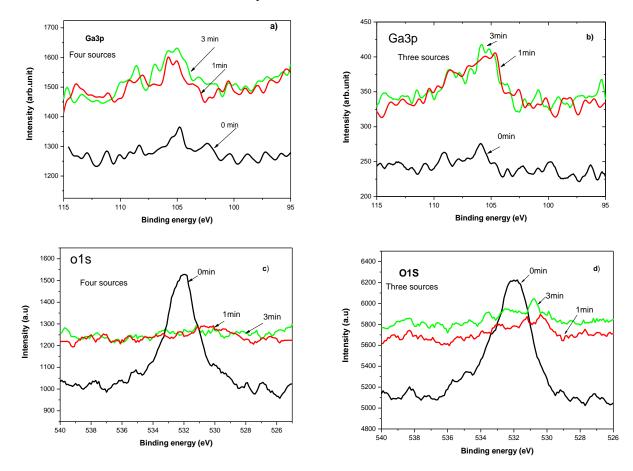

Fig. 3. XPS spectrum of Ga3p and O1s of CIGS film.s a), c) Four metal sources, b), d) Three metal sources

After 1mn of etching, the O1s peak has disappeared and no presence of oxygen is revealed. A depth profile of CIGS thin films was studied (no present here) and showed that the Ga concentration is homogenous in the CIGS bulk films. We can see that there is no significantchange in the binding energy of the elements study in the case of three and four metal sources. So, the good quality of the films does not depend of the number of evaporation sources. In order to study the effect of Ga on the behavior of the band gap of the CIGS according to the technical development , we present in Fig.4 the band gap variation as a function of Ga content (x=Ga/Ga+In) for various preparation methods. One can observe that the data variation tendency is similar for different synthesis processes and obeys the Vegards low:

$$E_g(x) = E_g^{CIS} + \left(E_g^{CGS} - E_g^{CIS}\right).x + b.x\,(1-x)$$

where b is the bowing parameter, E_g^{CIS} and E_g^{CGS} are the band gap for x= 0 (CIS) and x =1 (CGS) which are induces a difference with linear averaged behaviour (see inset Fig. 4).

The derived bowing factor for our measurements is 0.28 which is in good agreement with those reported in the literature from CIGS crystals [17], four sources coevaporated thin films [18] and thin films synthesised by bilayers technique [19]. The fit (red line) indicates that the bowing factor is around 0.20.
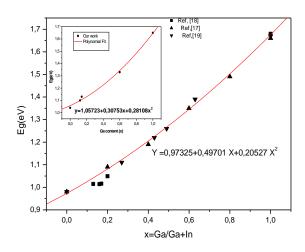
Fig. 4. Evolution of the band gap (Eg) of CIGS films as a function of Ga/Ga+In.

3.2. Electrical properties

Measurements of electrical conductivity CuIn$_{1-x}$Ga$_x$Se$_2$ thin films for 0.05≤x ≤0.23 were carried out using the Van Der Pauw method. Before measurements, gold electrodes were evaporated on CIGS films. The majority carrier type was studied by the hot probe technique and the CIGS layers are p-type. Fig.5 shows the variation of electrical conductivity (Lnσ) with temperature of CIGS thin films. It can be seen that the electrical conductivity varies from 2.4 10^{-2} to 0,5 Ω^{-1}.cm^{-1} at room temperature when x varies from 0.05 to 0.23 respectively. The results are similar to those reported by Guha et al. [18] for CIGS thin films obtained from four sources.

The conductivities of thin films with end compositions x= 0.05 and x= 0.23 were interpreted in terms of Werner model [20] introducing potential variations among different boundaries and modeling the fluctuating barrier ϕ by a Gaussian distribution:

$$P(\phi) = \frac{1}{\sigma_\phi \sqrt{2\pi}} exp\left(\frac{-(\overline{\Phi} - \phi)^2}{2\sigma_\phi{}^2}\right)$$

with $\overline{\Phi}$ mean barrier and σ_ϕ standard deviation. We obtain

$$\phi_{eff(T)} = \overline{\Phi}(T) - \frac{\sigma_\phi{}^2}{2KT/q}$$

The barrier Φ is replaced by an effective current barrier ϕ_{eff}. The second term of this equation results in a decrease of ϕ_{eff} upon cooling and consequently the slopes of Arrhenius plots of the conductivity are curved upwards. From fig.(6), a good agreement between the Werner theory and experimental data is observed.

Table 1. Electrical parameters of CIGS thin films

Ga/Ga+In	σ$_ø$ (meV)	$\overline{\Phi}$(meV)	H
x = 0.23	10,60	40,50	3,82
x = 0.05	7,10	23,72	3,34

The temperature dependence of the conductivity is well described by a parabola such as ln(σ/T)= ax^2+ bx + c with x =1/T (Fig. 6). The values of the standard deviation σø, the mean potential barrier height Φ(T = 0) are obtained from a and b. The homogeneity factor H is the ratio of Φ(T = 0)/σø. Their respective values are given in table 1. We can see that the Ga content affect the CIGS thin films quality when x varied from 0.05 to 0.23.
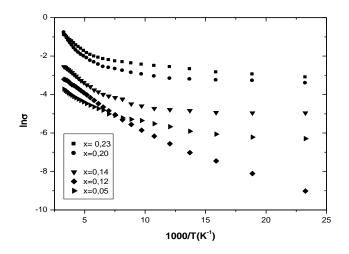

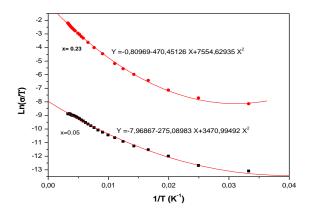*Fig. 5. Variation of the conductivity CIGS films v.s the reciprocal temperature*

Fig. 6. Temperature dependence of the conductivity in the temperature range 40–400 K of Cu(In$_{1-x}$Ga$_x$)Se$_2$ thin films

3.3. Photovoltaic characteristics

To study the current-voltage (I-V) data under standard conditions (100mWcm^{-2}, 25 °C), we exploited the formula [21]:

$$J = J_o \, exp\left[\frac{q(V - R_s J)}{AkT}\right] - J_o - J_L + \frac{V - R_s J}{R_{sh}}$$

where J_0 is the saturation current density. R_s, R_{sh} are series and shunt resistance. The ideality factor A and $J_L = J_{sc}$ at open circuit- voltage

Under illumination at $V = V_{oc}$ (J = 0), the equation above, can be transformed to

$$V_{OC} = Eg\frac{A}{2q} + \frac{AkT}{q}\ln\left[\frac{J_L}{J_{oo}}\right]$$

where J_{00} is a prefactor depend on voltage and room temperature (T).

The latter three sources (Cu +Ga, Cu+In, Se) coevaporated thin films are used to fabricate SLG/Mo/CIGS/In$_2$S$_3$/ZnO/Ni-Al solar cells for x = 0,14 - 0,28 and 0,60. The (I-V) characterization (Fig.7) under illumination exhibit a diode behavior and the derived efficiency is given see inset fig.7; where Voc is the open circuit voltage, FF the fill factor, Jsc is the short-current density and η is the efficiency.
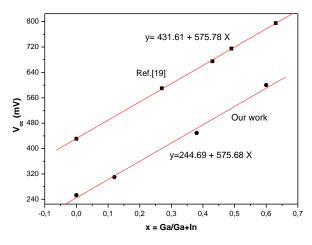

Fig. 7. J-V characteristics of Mo/Cu(In$_{1-x}$Ga$_x$)Se$_2$/In$_2$S$_3$/ ZnO/NiAl solar cells (x = 0.14; 0.2; 0.6).

It is noted that the efficiency depends considerably of the interface CIGS thin films absorber and the (In$_2$S$_3$) buffer layers. Furthermore, one can notice the V$_{oc}$ increases when the Ga content increases as observed in Fig. 8. This effect of the V$_{oc}$ is also observed by Malmström et al. [19] for CIGS thin films obtain by four sources coevaporation. On the other hand, one can expect the same behavior for the variation of V$_{oc}$ as a function of band gap (Fig. 9). This confirmation data is reported by H.W. Shock et al. [22] when Eg is less than 1.4 eV. This indicates that the increase of V$_{oc}$ can be explained by a

reduction of the back-interface recombination velocity [23] with increasing back-side Ga gradient.
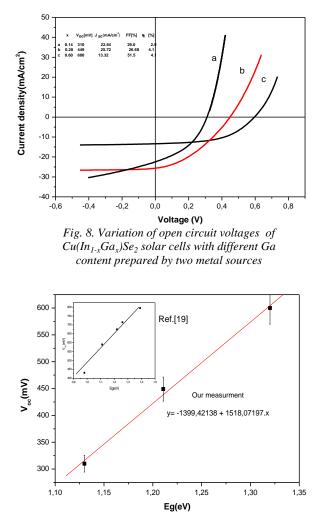

Fig. 8. Variation of open circuit voltages of Cu(In$_{1-x}$Ga$_x$)Se$_2$ solar cells with different Ga content prepared by two metal sources

Fig. 9. Plot of the open circuit voltage V$_{oc}$ vs. the bang gap energy (Eg). The red line   corresponds to a linear fit with a fixed slope

3.4. Conclusion

The XRD revealed that the synthesis of CIGS thin films was successfully achieved using three evaporation metal sources. The XPS study confirmed that the bulk quality of the obtained layers is not affected by oxygen. The derived bowing factor of our materials is comparable with that reported in the literature for four sources. The conductivity measurements showed that transport process in the synthesized thin films is governed by the grain boundary scattering mechanism.   The current-voltage study showed that the open circuit voltage presents a linear variation as a function of Ga content in both three and four deposited thin films. The low derived efficiency is mainly attributed to the mechanism CIGS/buffer layer interface since the physico-chemical properties of the achieved three sources thin films are satisfactory and are

comparable with those obtained by four sources evaporation.

References

[1] Z. Han, D. Zhang, Q. Chen, R. Hong, C. Tao, Y. Huang, Z. Ni, S. Zhuang, Mater. Res. Bull. **51**, 302 (2014).

[2] D. Nam, S. Jung, S. Ahn, J. Gwak, K. Yoon, J. H. Yun, H. Cheong, Thin Solid Films **535**, 118 (2013).

[3] J. Philip, H. Dimitrios, L. Erwin, P. Stefan, W. Roland, M. Richard, W. Wiltraud, P. Michael, Progress in Photovoltaics: Research and Applications **19**, 894 (2011).

[4] S. Viswanathan, Saji, Ik-Ho Choi, Chi-Woo Lee, Solar Energy **85**, 2666 (2011).

[5] A. Chirila, P. Reinhard, F. Pianezzi, P. Bloesch, A. R. Uhl, C. Fella, L. Kranz, D. Keller, C. Gretener, H. Hagendorfer, D. Jaeger, R. Erni, S. Nishiwaki, S. Buecheler, A. N. Tiwari, Nature Materials **12**, 1107 (2013).

[6] P. Jackson, D. Hariskos, E. Lotter, S. Paetel, R. Wuerz, R. Menner, W. Wis-chmann, M. Powalla, Progress in Photovoltaics: Research and Applications **19**, 894 (2011)

[7] Philip Jackson, Dimitrios Hariskos, Roland Wuerz, Wiltraud Wischmann, Michael Powalla, Phys. Status Solidi RRL **8**(3), 219 (2014).

[8] Miguel A. Contreras , Manuel J. Romero, R. Noufi, Thin Solid Films **511**, 51 (2006).

[9] A. Drici, M. Mekhnache, A. Bouraoui, A. Kachouane, J. C. Bernède, A. Amara, M. Guerioune, Materials Chemistry and Physics **110,** 76 (2008).

[10] L. Assmann, J. C. Bernède, A. Drici, C. Amory, E. Halgand, M. Morsli, Applied Surface Science **246,** 159 (2005).

[11] N. Barreau, J.C. Bernède, S. Marsillac, A. Mokrani, J. Cryst. Growth, **235,** 439 (2002).

[12] X. Ji, L. J. Wang, J. Y. Teng, Y. I. M. Mi, C. M. Zhan, J. Optoelectron. Adv. M. **17**, 1710 (2015).

[13] M. A. Contreras, K. Ramanathan, J. AbuShama, F. Hasoon, D. L. Young, B. Egaas, R. Noufi, Prog. Photovolt: Res. Appl. **13,** 209 (2005).

[14] K. Ramanathan, M. A. Contreras, C. L. Perkins, S. Asher, F. S. Hasoon, J. Keane, D. Young, M. Romero, W. Metzger, R. Noufi, J. S. Ward, A. Duda, Prog. Photovolt: Res. Appl. **11,** 225 (2003).

[15] R. Caballero, C. A. Kaufmann, V. Efimova, T. Rissom, V. Hoffmann, H. W. Schock, Progress in Photovoltaics: Research andApplications **21**, 30 (2013).

[16] R. Caballeroa, C. Maffiotte, C. Guillén, Thin Solid Films **474**, 70 (2005).

[17] C. A. Durante Rincón, E. Hernández , M. I. Alonso, M. Garriga, S. M. Wasim, C. Rincón, M. León, Materials Chemistry and Physics **70**, 300 (2001).

[18] P. Guha, S. N. Kundu, S. Chaudhuri, A. K. Pal, Materials Chemistry and Physics **74,** 192 (2002).

[19] J. Malmström, J. Wennerberg, M. Bodegård, L. Stolt, Seventeenth European Photovoltaic Solar Energy Conference: Proceedings of the International Conference held in Munich, Germany 22-26 October 2001, 1265 (2001).

[20] J. H. Werner, H. H. Guttler, J. Appl. Phys. **69,** 1522 (1991).

[21] R. Scheer, H. -W. Schock, "Thin film heterostructures," in Chalcogenide Photovoltaics, Weinheim, Germany: Wiley-VHC, (2011) p. 9.

[22] H. W. Schock, U. Rau, T. Dullweber, G. Hanna, M. Balboul, T. Margorian-Friedlmeier, H. Wiesner, In Proceedings of the 16th European Photovoltaic Solar Energy Conference **1**, 304 (2000).

[23] V. Gremenok, V. Zalesski, A. Khodin, O. Ermakov, R. Chyhir, V. Emelyanov, V. Syakersky, physica status solidi (c) **6**, 1237 (2009).

_____

[*]Corresponding author: abdelaziz.drici@univ-annaba.org